

Towards an accurate description of an accretion induced collapse and the associated ejected mass

Amir Sharon¹^{*} and Doron Kushnir¹

¹*Dept. of Particle Phys. & Astrophys., Weizmann Institute of Science, Rehovot 76100, Israel*

Accepted XXX. Received YYY; in original form ZZZ

ABSTRACT

We revisit the accretion induced collapse (AIC) process, in which a white dwarf collapses into a neutron star. We are motivated by the persistent radio source associated with the fast radio burst 121102, which was explained by Waxman (2017) as a weak stellar explosion with a small ($\sim 10^{-5}M_{\odot}$) mass ejection. Since a typical supernova ejects much larger amount of mass, we study the possibility that an AIC caused the weak explosion. Additionally, the interaction of the relatively low ejected mass with a pre-collapse wind might be related to fast optical transients. The AIC is simulated with a one-dimensional, Lagrangian, Newtonian hydrodynamic code, and we put an emphasis on accurately treating the equation of state and the nuclear reaction network. We leave subjects such as neutrino physics and general relativity corrections for future work. Using an existing initial profile and our own initial profiles, we find that the ejected mass is $\sim 10^{-2} - 10^{-1}M_{\odot}$ over a wide range of parameters, and construct a simple model to explain our results. Our results probably provide an upper limit to the ejected mass from AIC events.

Key words: hydrodynamics – white dwarfs – stars: neutron

1 INTRODUCTION

Accretion induced collapse (AIC) is a theorized process in which a white dwarf (WD) collapses into a neutron star (NS), followed by an explosion that ejects a fraction of the star’s mass at mildly relativistic velocities. AIC has been proposed as the outcome of an accreting WD and as a possible NS formation channel (Canal et al. 1980; Nomoto 1986). Existence of young pulsars in globular clusters (Lyne et al. 1996) suggests that some fraction of NSs indeed created in this way. A renewed interest in this process has arisen recently, following new astronomical discoveries that may be related (Waxman 2017; Lyutikov & Toonen 2018).

One discovery that may be related to AIC is the persistent radio source associated with FRB 121102 (Scholz et al. 2016). The FRB source resides in a dwarf galaxy at a distance of ~ 970 Mpc, with a persistent radio source located in that direction (Chatterjee et al. 2017). According to Waxman (2017), the persistent radio source was created by a weak stellar explosion, and a possible scenario to explain this event is an AIC, with the resulting NS acting as the source of the FRBs.

Another window for observing AIC might be fast-rising blue optical transients (Drout et al. 2014). The interaction

of the ejected mass with a pre-collapse wind could be related to these events (Lyutikov & Toonen 2018), that are characterized by a short optical rise time, < 10 days, and a peak luminosity comparable to supernovae.

The AIC process is the consequence of a WD, which is being held mostly by electron degeneracy pressure, that accumulates enough mass to surpass the Chandrasekhar mass limit, M_{Ch} , at which point it can no longer support its own mass and collapses. The WD collapses over its own free-fall time, $t_{ff} \sim 0.1$ s, until the core reaches nuclear densities ($\rho_{nuc} \sim 10^{14}$ g cm⁻³) and repelling strong interactions halt the collapse. The radius of the core at bounce is:

$$R \approx \left(\frac{3}{4\pi} \frac{M_{Ch}}{\rho_{nuc}} \right)^{1/3} \cong 20 \text{ km}, \quad (1)$$

roughly a factor of 5 larger than the Schwarzschild radius, $r_s = 2GM_{Ch}/c^2 \cong 4$ km. The characteristic velocity of the ejected material is comparable to the escape velocity, $v_{esc} = \sqrt{r_s/Rc} \cong 0.5c$, and is mildly relativistic. The gravitational energy per baryon around the core is:

$$\epsilon \sim \frac{3GM_{Ch}}{5R} \sim 50 \text{ MeV/baryon}, \quad (2)$$

which is converted to internal and kinetic energy, corresponding to a temperature of $T \lesssim 5 \times 10^{11}$ K. During the collapse, the outer layers bounce off the dense core, creating

* E-mail: amirsha@weizmann.ac.il

a shock wave that propagates outwards, ejecting some mass in the process. Since most of the gravitational energy is converted to internal energy, only some fraction of the initial mass will be ejected, while the remaining core becomes a NS.

Simulating AIC raises some challenges that should be carefully addressed. The range of densities and temperatures throughout the process varies greatly, from nuclear densities ($\rho_{nuc} \sim 10^{14} \text{ g cm}^{-3}$) at core bounce to very low densities ($< 10^5 \text{ g cm}^{-3}$) at the edge of the star. The entire range should be described accurately and smoothly by the equation of state (EOS). The high temperatures and densities cause nuclear reactions to be very rapid, and these reactions should be treated in a self-consistent way. Neutrinos play an important part in the process (Woosley & Baron 1992), and general relativity (GR) corrections should also be accounted for, as the radius of the core after bounce is comparable to the Schwarzschild radius.

Several previous studies have estimated the amount of ejected mass from an AIC (Woosley & Baron 1992; Fryer et al. 1999; Dessart et al. 2006). Woosley & Baron (1992) estimated an ejected mass of $M_{ej} \sim 0.01 M_{\odot}$, using a progenitor made by Nomoto (1986), and one-dimensional (1D) hydrodynamic simulations that include neutrino transport. Fryer et al. (1999) considered the effects of neutrino physics and employed different EOS, and found the ejected mass to be $M_{ej} \sim 0.2 M_{\odot}$ in most of their simulations. They further found that, except for the EOS, most parameters (neutrino physics, general relativity) do not significantly change the results. In their simulations, the ejecta has a low electron fraction Y_e . Considering the low Y_e values of the ejected mass, they used the abundance of heavy elements in the Galaxy to derive an upper limit on the AIC rate in the Galaxy of $\sim 10^{-5} \text{ yr}^{-1}$. Dessart et al. (2006) performed multidimensional simulations and found an ejected mass of $M_{ej} \sim 10^{-3} M_{\odot}$, with a typical velocity of $\sim 0.1c$. The reason for the discrepant results between the different works is not entirely clear. However, the different hydrodynamic schemes and EOS might be a significant source of uncertainty in these studies and one of the reasons for the different results. These works either assumed the entire star to be in nuclear statistical equilibrium (NSE) and did not include a nuclear reaction network (Fryer et al. 1999; Dessart et al. 2006), or flash-burned the matter to NSE (Woosley & Baron 1992). Nuclear burning is important in order to have a star with appropriate initial conditions that will successfully collapse in a feasible manner. Having the entire star at NSE prior to collapse is unrealistic, since the density and temperature near the edge are far below NSE conditions. Nuclear burning is required for matter originally not in NSE to have a smooth transition to NSE when the temperature is high enough. If nuclear burning is not enabled and the composition for some part of the star is fixed, the EOS will eventually fail to describe the matter when its density becomes high enough for nuclear interactions to be important ($\rho \gtrsim 10^{11} \text{ g cm}^{-3}$).

We aim in this paper to provide an accurate numerical calculation of an AIC (for given initial conditions and input physics) for the spherical case, where neutrinos and GR corrections are neglected. We use a 1D, Lagrangian, Newtonian hydrodynamics scheme, and focus on an accurate treatment of the EOS and the nuclear reaction network, in order to resolve the uncertainties associated with these param-

eters. For this purpose, the preparation of a relevant EOS for several regimes (of density, temperature, composition) is required, and the different regimes should be smoothly connected. Our solution for this case may serve as the foundation for adding more physical processes, such as the effect of deleptonization and neutrinos, GR corrections, rotation and additional dimensions. Calculations were done with the VULCAN 1D hydrodynamic code (Livne 1993), together with MESA routines for the EOS and for the nuclear reaction network (Paxton et al. 2010, 2015), modified for our purposes.

The structure of the paper is as follows: In section 2, we describe the hydrodynamic scheme we use for the simulations. Section 3 describes our attempts to reproduce the results of Fryer et al. (1999). In section 4, we describe the results of simulations with our own initial profiles. In section 5, we propose a simple model to describe the outcome of the collapse for isentropic initial profiles. In appendix A, we provide additional numerical details regarding the scheme, while appendix B contains a comparison with an analytic solution of the collapse for an ideal gas polytrope (Yahil 1983).

2 METHODS

We use the 1D Lagrangian hydrodynamics code VULCAN 1D (Livne 1993) along with our modifications. One such modification is replacing the energy with the entropy as an EOS variable. The reason is that the electrons, which contribute most of the pressure, are highly degenerate, and therefore small deviations in the energy can lead to large fluctuations in the temperature. For more details, see Appendix A2.

The EOS consists of a few terms: electron-positron plasma, radiation, nuclei, nuclear level excitations and Coulomb corrections, where full ionization is assumed at all times. The electrons and positrons are treated with the Timmes EOS (Timmes & Arnett 1999) at all regimes. At low densities ($\rho \ll 10^{11} \text{ g cm}^{-3}$), nuclei are treated as an ideal gas mixture, described by the density, ρ , the specific entropy, s , and the mass fraction of each isotope, X_i . We use the MESA routines (Paxton et al. 2010) for the EOS of the ions at low densities and for the Coulomb corrections, with some modifications, to accurately describe the entropy (for more details, see Kushnir (2018)). Coulomb corrections are based on Chabrier & Potekhin (1998). It is important to include all isotopes with non-negligible mass fractions at the densities and temperatures where the MESA EOS is active. We have found that a list of 183 isotopes is sufficient (for more details about the isotope selection process, see A1).

The ions are assumed to be in nuclear statistical equilibrium (NSE) at high temperatures and low densities, with the composition being determined by the density, ρ , entropy, s and electron fraction, Y_e . At this regime, and at high densities, a tabulated EOS, which describes matter in NSE and at nuclear densities is used (see appendix A1 for more details).

As densities approach $\sim 10^{11} \text{ g cm}^{-3}$, nuclear interactions become important and the ions can no longer be treated as an ideal gas. For these regimes, we use the tables and routines provided in stellarcollapse.org/microphysics (O'Connor & Ott 2010; Schneider et al. 2017). These ta-

bles use nuclear EOS (Lattimer & Swesty 1991; Shen et al. 2011b,a), and as in the NSE case, receive the triplet (ρ, s, Y_e) and return the rest of the variables. As the density approaches nuclear densities ($\sim 10^{14} \text{ g cm}^{-3}$), these EOS become stiff, although there is some variability in modelling the transition to nuclear densities (Lattimer 2012). The routines provided by Schneider et al. (2017) allow the creation of an EOS table for matter in NSE and a table for nuclear EOS using the single nucleus approximation (Lattimer & Swesty 1991) and their merger in a thermodynamically consistent manner. We have made some modifications in these routines to fit smoothly to the modified MESA EOS, such as the Coulomb correction term. When the EOS of O'Connor & Ott (2010) are used, the entire table is provided in advance with no editing option, so the transition between the MESA and the tabulated nuclear EOS is not guaranteed to be smooth.

At the low temperature and density regimes, nuclear burning takes place and is implemented using the MESA routines (Paxton et al. 2015), with raw reaction rates taken from the JINA reaclib database (Cyburt et al. 2010). Neutrino physics is based on the deleptonization scheme of Liebendörfer (2005) and the thermal neutrino creation of Itoh et al. (1996). For more details, see appendix A1 and A3.

3 REPRODUCING PREVIOUS RESULTS

In order to test our scheme, we compared our results with the analytic solution of Yahil (1983), which describes the collapse of a star with a polytrope EOS. This solution is quite relevant, since a complicated EOS can be approximated as polytropes under some conditions (mainly due to the degeneracy of the electrons). The simulation results deviate by less than 6% from the analytic solution over a range of 10 orders of magnitude. More details regarding the comparison to the analytic solution are given in appendix B.

We next tried to reproduce the results of Fryer et al. (1999) for their initial profile (taken from Woosley & Baron (1992)). This initial profile is taken in the midst of the collapse, where all parts of the star have already begun falling towards the center. The inner part of the star, up to an enclosed mass of $m = 0.54M_{\text{tot}}$, where M_{tot} is the total mass of the profile, is in NSE and has gone through some deleptonization, with Y_e starting at ~ 0.4 at the center and linearly increasing with the mass until it reaches 0.5 at the edge of the inner part. For $m > 0.54M_{\text{tot}}$, the star has not gone through nuclear burning or deleptonization. There, the composition is divided equally between carbon and oxygen (CO) until $m = 0.82M_{\text{tot}}$, and the outer layers of the star are composed of helium. The temperature at the boundary of the NSE and non-NSE regions sharply drops from $\sim 9 \times 10^9 \text{ K}$ to $\sim 2 \times 10^7 \text{ K}$, since the nuclear reactions that had taken place at the inner parts of the star contribute energy to these parts and increase their temperature. Fryer et al. (1999) ran this initial profile for 0.2s, testing the sensitivity to several parameters, such as the EOS and neutrino physics.

We tried to reproduce a run where the EOS used for the high densities was the Lattimer Swesty (LS) EOS, with an incompressibility of the bulk nuclear matter parameter of $K_S = 180 \text{ MeV}$, and without any neutrino treatment, for

which Fryer et al. (1999) had obtained an ejected mass of $0.2 M_{\odot}$. There were several issues we encountered while trying to reproduce these results. The original profile used in Woosley & Baron (1992) and in Fryer et al. (1999) could not be found¹. Nevertheless, a similar profile was kindly provided to us by Eddie Baron. This profile did not exactly match the original profile, as the central density, radius and maximum collapse speed of the profile we were given are $4.05 \times 10^{10} \text{ g cm}^{-3}$, $1.1 \times 10^8 \text{ cm}$ and $3.2 \times 10^8 \text{ cm s}^{-1}$ compared to $6.53 \times 10^{10} \text{ g cm}^{-3}$, $0.96 \times 10^8 \text{ cm}$ and $3.0 \times 10^8 \text{ cm s}^{-1}$, respectively. Additionally, the innermost region of the part of the star which is not in NSE, from $m = 0.55M_{\text{tot}}$ up to $m = 0.58M_{\text{tot}}$, has negative entropy according to our MESA EOS. This is due to the degeneracy of the ions, which the MESA EOS does not handle, as it assumes the ions are composed of an ideal gas. We have not modified this region, as the negative entropy does not interrupt the execution of the EOS. For these low densities, Fryer et al. (1999) assumed that the composition is in NSE at all times (it is unclear to us how this was implemented with an initial profile starting at a certain non-NSE composition).

We ran this profile with our scheme, using the LS EOS for the high-density regime and NSE for high temperatures and low densities, with nuclear burning taking place, and no neutrinos. The entropy in the region that is initially negative quickly rises to positive values due to nuclear burning and small shock waves. The obtained ejected mass in our calculations is $\approx 0.173M_{\odot}$, with this number converging for a resolution of 400 cells or higher, with the cells divided such that the resolution around the mass cut (the Lagrangian mass coordinate separating the star and the ejecta) is increased. This is within 15% of the results of Fryer et al. (1999), despite all the issues we encountered. We have also used the LS220/NSE EOS for this profile. Results for this EOS were $\approx 0.095M_{\odot}$, about half the amount of the LS180 EOS, which demonstrates the impact of the EOS on the ejected mass.

4 A PARAMETER STUDY

The initial profile of a collapsing WD has many parameters that can affect the ejected mass, such as the mass, composition, temperature profile and electron fraction. We do not aim here to determine what is the initial profile, but instead we parametrize a few initial profiles in order to provide an estimate for the range of possible ejected mass during AIC.

Our initial profiles consist of an isentropic Chandrasekhar mass star in a hydrostatic equilibrium with most of its mass having an adiabatic index below 4/3. In order to construct such a profile, we adopted some of the properties of the initial profile from the previous section. It is assumed that the inner parts of the star have gone through nuclear burning and some deleptonization and are in NSE, with the electron fraction, Y_e , starting at some value $Y_e(0)$ at the center and rising linearly with the mass until it is 0.5 at about $m = 0.65M_{\text{tot}}$. Constructing the profile is done inside-out, where the density, pressure, temperature and other thermodynamic quantities are determined from hydrostatic equilibrium and the predetermined entropy and electron fraction.

¹ We thank Chris Fryer and Stan Woosley for their effort to locate this profile.

As the distance from the center increases, the temperature decreases until it crosses a threshold $T_{\text{thr}} = 9 \times 10^9$ K, after which it is assumed that nuclear burning is negligible. In this region, the temperature drops to 2×10^8 K and the mass fraction is equally divided between carbon and oxygen. The entropy of the outer parts also drops by a constant factor, determined by the ratio between the entropy before the temperature drops and afterwards, taken with the density at the transition. The initial entropy is chosen such that the total mass of the star is the Chandrasekhar mass.

The star is driven to collapse by giving its layers initial infall velocities or reducing the pressure in the center. Since the adiabatic index is lower than $4/3$, the collapse continues until the EOS stiffens. An external pressure is applied to the star to maintain the hydrostatic condition at the beginning of the run, and is kept constant until bounce. After bounce and expansion, as the pressure of the ejecta becomes smaller as it expands, the external pressure is modified so that the expansion will continue smoothly.

4.1 A specific example

The collapse of one specific profile is shown in Figure 1. The nuclear EOS used in the run was the LS220/NSE EOS, created from the routines of Schneider et al. (2017). The initial density and electron fraction at the center were $5 \times 10^{10} \text{ g cm}^{-3}$ and 0.4, respectively. The uniform initial entropy per baryon was $1.72 k_B^{-1}$ and the resolution was 400 cells, divided with equal radial spacing. We did not include deleptonization, and the whole Y_e profile (as a function of mass) was kept constant throughout the collapse. Panel (a) of Figure 1 shows the trajectory of chosen mass elements, and panel (b) of Figure 1 shows the total specific energy (gravitational, kinetic and internal) of the mass elements, taken at several snapshots (before the collapse, at the time of bounce, during the shock propagation and after the shock breakout). The ejected mass of this run is $2.84 \times 10^{-2} M_\odot$, which can be read from the point where the energy curve intersects with the x axis, showing the amount of mass with positive energy. The typical energies of the ejecta are tens of MeV/baryon, with the outermost shells rising above 100 MeV/baryon. These energies correspond to mildly relativistic velocities of about $0.15 - 0.3c$ for most of the ejected mass. The ejecta is composed mainly of ^{56}Ni , since it is the most abundant isotope of matter in NSE at low temperatures and $Y_e = 0.5$. Some mass elements started moving outwards before bounce, seen at $t \approx -10$ ms in Figure 1a. This is due to the energy gained by nuclear burning, causing these elements to reverse their motion before bounce. After bounce, they are quickly caught up by the emerging shock, which moves at much higher velocities (note that the energy gained by the difference of the gravitational binding energy is tens of MeV/baryon, an order of magnitude higher than the typical nuclear binding energy of \sim MeV/baryon).

In order to check convergence, we examined additional scenarios, where resolution was altered while the rest of the parameters remained the same. The resolution increased up to 988 cells that were divided in the same manner. Figure 2 shows the convergence of the run, by plotting, as a function of the resolution, the divergence of the ejected mass from that of the run with the 988 cells (where the ejected mass was $0.0285 M_\odot$). For resolutions higher than 200 cells, the

the deviation of the calculated ejected mass from that of the highest resolution does not exceed $3 \times 10^{-4} M_\odot$, reflecting a 1% error.

4.2 Varying the EOS and initial conditions

In order to assess the effects of the EOS and initial conditions, we calculated the ejected mass for several nuclear EOS and uniform initial entropy values. The ejected mass in these runs is provided in Figure 3. The LS220/NSE and SKRA/NSE EOSs are created from the routines of Schneider et al. (2017) with different nuclear parameters, and the EOS of HShen and GShen are taken from O'Connor & Ott (2010). The LS180 EOS used in the previous section is not part of the list of EOS used here, because its parameters, and specifically the incompressibility of the bulk nuclear matter being $K_S = 180$ MeV, are currently not favoured (Lattimer 2012). Also shown are runs where the entire star is in NSE and there is no nuclear reaction network, along with a model estimate, which is discussed in section 5.

The ejected masses are plotted as a function of the uniform initial entropy, all starting with a central density of $5 \times 10^{10} \text{ g cm}^{-3}$. Note that for each value of the initial entropy there is a value for the central electron fraction $Y_{e,c}$ that ensures the mass of the star to remain the Chandrasekhar mass. Since the pressure rises with the entropy and with $Y_{e,c}$, the electron fraction should be decreased for a larger initial entropy in order to keep the mass of the star unchanged. As in the previous section, deleptonization is not included. The ejected mass in all runs is $\text{few} \times 10^{-2} M_\odot$. The EOS and initial entropy alters the ejected mass by a factor of a few, but does not change it by orders of magnitude.

The initial profile also has a considerable effect, as the results of this section are smaller by a factor of a few than the results in section 3, where the ejected mass is $\approx 0.095 M_\odot$ for the LS220/NSE EOS. To explain this discrepancy, we attempted to build a hydrostatic initial profile with the same temperature-entropy structure as in the initial profile in Section 3 (which is not isentropic). The total mass in the initial profile we built, using the LS220/NSE EOS, was $\sim 0.05 M_\odot$ less than the Chandrasekhar mass of the original profile, with this mass deficiency affecting the density profile at the outer parts of the star. The cause for this discrepancy is the hydrostatic equilibrium requirement that does not hold for the original profile. The ejected mass of our own hydrostatic profile was about $0.025 M_\odot$, similar to the results in Figure 3 for the LS220/NSE EOS. Since the ejected mass of the original profile is $\sim 0.095 M_\odot$ (see 3), the progenitor mass difference of $0.05 M_\odot$ between the initial profiles might be the reason for the difference in ejected masses.

4.3 Effects of neutrinos

The obtained range of ejected mass is probably an upper limit, since neutrino creation and emission, which are not taken into account in the previous simulations, will lead to energy and entropy losses, making it more difficult for the mass shells to escape from the star (on the other hand, the neutrinos can deposit some of the energy back when interacting with the outer layers, before escaping the star). To

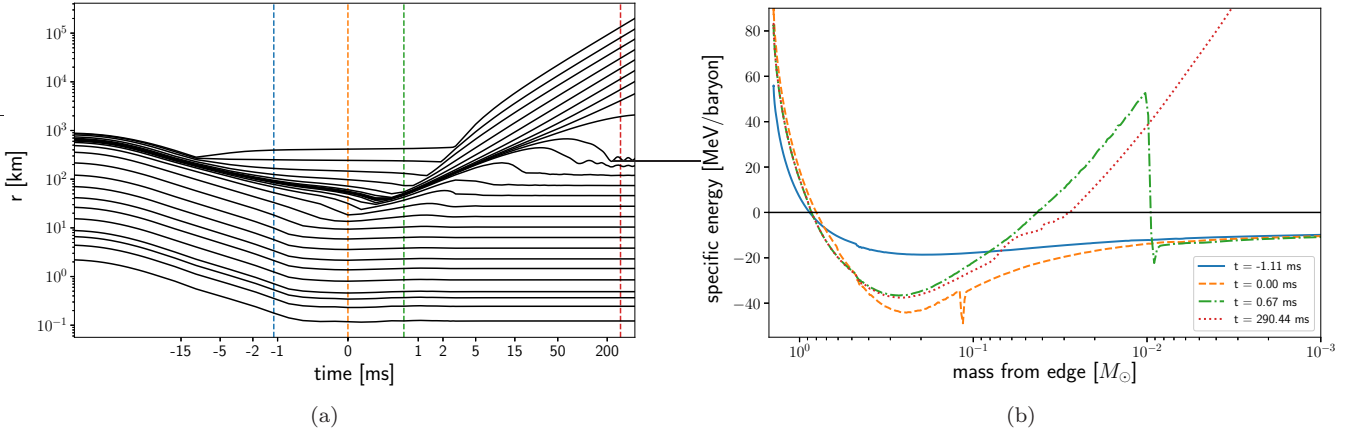


Figure 1. Collapse of a custom profile of a Chandrasekhar mass WD, made with the LS220/NSE EOS, no neutrino treatment and a resolution of 400 cells. The initial profile is isentropic, with an entropy of $1.72 k_B^{-1}$. (a) Trajectories of chosen mass elements. The x axis scale is symmetrical logarithmic, with a linear range at $t \in [-1 \text{ ms}, 1 \text{ ms}]$, where time is measured relative to the time of bounce. (b) Total specific energy of mass elements at different times, plotted as a function of the mass from the edge of the star. The vertical lines in panel (a) indicate the time of the curves in panel (b). These times occur before the collapse (blue), at the time of bounce (orange), during the shock propagation (green) and after the shock breakout (red). The ejected mass of the collapse is calculated by the amount of mass with positive energy, which can be seen by the intersection of the energy curve with the x axis at late times.

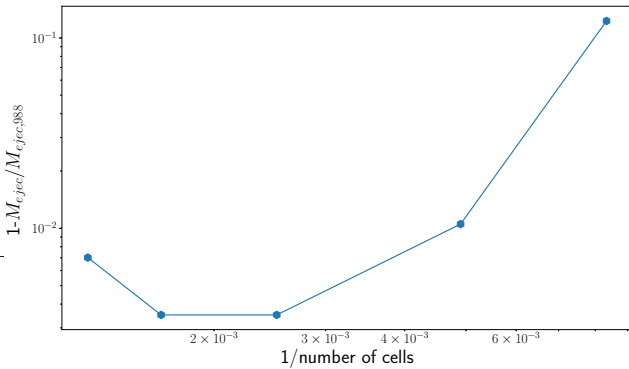


Figure 2. Deviation of the ejected mass from the highest resolution run with 988 cells (emitting $0.0285 M_\odot$), as a function of the resolution. The parameters of the runs (except the number of cells) are the same as in Figure 1. For resolutions higher than 200 cells, the error is within 1%.

grasp the effect of the neutrinos, we tested the case where the neutrinos only carry energy away without any additional interaction (see appendix A3). The addition of neutrinos emission, mainly due to deleptonization, leads to a reduction in the ejected mass by roughly an order of magnitude, to $\sim 10^{-3} M_\odot$. This can be considered a lower limit for these profiles, EOS and input physics. Other parameters, such as general relativity, might further reduce the ejecta mass.

5 A SIMPLE ESTIMATE OF THE EJECTED MASS

We now construct a simple model to describe the structure of the proto-neutron star (PNS) at the end of the collapse and to evaluate the ejected mass. We assume that the tabulated EOS, which describes nuclear matter for high densities and ideal gas in NSE for low densities, can be used for the entire

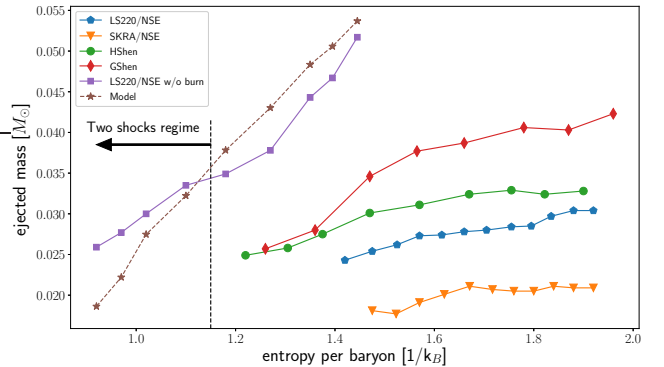


Figure 3. Ejected mass for various EOS and initial entropy values (solid lines). Also shown are runs with no burning (purple) and the model estimates for these runs (brown dashed line). All profiles have the Chandrasekhar mass and a central density of $5 \times 10^{10} \text{ g cm}^{-3}$. The ejected mass in all runs is a few $\times 10^{-2} M_\odot$. The model is not valid in the low ejecta region, where another shock is created from infalling matter that further heats the outer layers of the star.

star. We therefore assume that the matter is in NSE and that there is no burning, and we neglect neutrinos. Another assumption is, as in the previous section, that the initial profile is isentropic. We assume that the flow is isentropic throughout the collapse, until the matter is shock-heated by the shock that was created from the bounce of the infalling matter, which alters the entropy profile, resulting in hydrostatic equilibrium. The model requires two unknown parameters - the central density of the final hydrostatic star ρ_{static} , and the (larger) central density at the time of bounce, ρ_{bounce} , which is used in order to estimate the shock strength. The two parameters, together with the hydrostatic equilibrium and isentropic flow conditions above, are sufficient to construct the PNS. The two parameters are retrieved from the numerical simulations in the previous section. Figure 4 shows

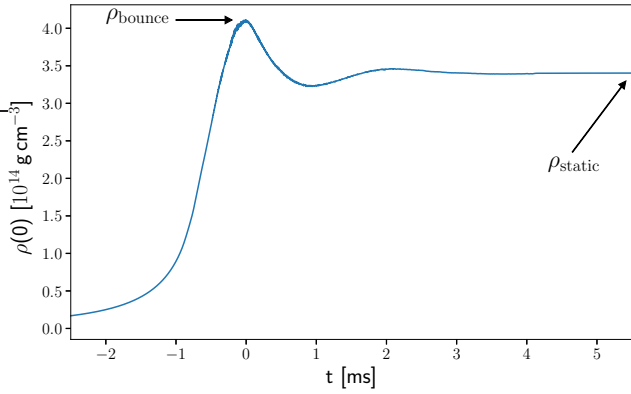


Figure 4. Central density as a function of time for a typical simulation run. The two unknown parameters of the model, the central density at bounce and the central density of the hydrostatic star are marked.

the central density as a function of time for a typical run, and how we extracted the density of the hydrostatic star and at bounce that we used in the model. The ejected mass can be calculated from the difference in mass between the initial WD and the PNS.

To begin constructing a hydrostatic star, the central density, ρ_{static} , and entropy (or any other two thermodynamic variables, given an EOS) should be predetermined. The latter is determined from the initial entropy, while the former, as afore mentioned, is extracted from the simulation result. The final central density can be approximately estimated as the nuclear density, but the ejected mass was found to be quite sensitive to this value, changing by 10 – 30% as a result of a 5% change in the density. The density-pressure profile is then determined from the hydrostatic equilibrium,

$$\frac{\partial p}{\partial r} = -\frac{Gm\rho}{r^2}, \quad (3)$$

and the shock heating. To estimate the shock heating, we assume that the infalling matter bounced and immediately stopped; hence, the strength of the shock will be determined out of the infall velocity, u , through the Hugoniot conditions,

$$u^2 = (p_1 - p_0)(V_0 - V_1) \quad (4)$$

$$\epsilon_1 - \epsilon_0 = \frac{1}{2}(p_1 + p_0)(V_0 - V_1), \quad (5)$$

where $V = 1/\rho$ and the 0 and 1 subscript refer to the upstream and downstream, respectively. Once the infall velocity is known, it is possible to retrieve all the variables using the conditions mentioned above.

To estimate the infall velocity, we make use of the self-similar solution discussed in Appendix B. The velocity is given by:

$$u = \kappa^{\frac{1}{2}} G^{\frac{1-\gamma}{2}} (t_c - t_{\text{bounce}})^{1-\gamma} U(X), \quad (6)$$

where $\kappa = p/\rho^\gamma$, X, U are the known self-similar coordinate and velocity, respectively, and $t_c - t_{\text{bounce}}$ is the time from bounce (for the self-similar solution, the density diverges at t_c). The adiabatic index γ and the constant κ are determined from the EOS at the given initial entropy and an averaged value of Y_e . The quantity $t_c - t_{\text{bounce}}$ is related to the second unknown parameter - the central density at bounce - by

using the (known) self-similar density:

$$D(0) = G(t_c - t_{\text{bounce}})^2 \rho_{\text{bounce}}. \quad (7)$$

In such a way, the velocity can be obtained given the radius, r , and the PNS can be constructed.

We note that the quantity $t_c - t_{\text{bounce}}$ can be roughly estimated by comparing the final central density (the first parameter) to the self-similar density using the same relation, Equation (7), but this gives an over estimate of $t_c - t$, since the density of the end state is not as high as it was at the time of the bounce and shock formation. This will result in a weaker shock and lower temperatures and pressures, which can support less mass, leading to a higher ejected mass. The estimation of $t_c - t_{\text{bounce}}$ from ρ_{bounce} is not entirely optimal, but gives the correct ejected mass to within 15%, where in some cases the difference is less than 5%. When the initial entropy decreases and the ejected mass becomes low ($\lesssim 0.035M_\odot$), some of the matter being ejected by the shock falls back into the star. When it meets the star, another shock wave is created, which further increases the entropy of this matter. This effect is not captured in our model, so the estimates for the runs with low initial entropy give a lower mass compared to the simulations.

Figure 3 shows the simulation results and the model estimations for profiles with the LS220/NSE EOS and an initial central density of $5 \times 10^{10} \text{ g cm}^{-3}$. The regime of ejected mass where the second shock is significant is marked, and the model's deviations grow substantially. Since the model calculates the ejecta from the mass difference between the two stars, it is valid only because the ejecta is not a very small fraction of the star, about 2–5%. For an ejecta of 5% of the star, an error of 1% of the mass of the PNS would result in an error of 20%, and will increase as the ejecta becomes a smaller fraction. If the range of ejected mass would have been an order of magnitude smaller, the accuracy of the model would have to be high enough to calculate the mass of the PNS within $< 0.1\%$ in order to have reasonable results.

Figure 5 compares the energy and entropy profiles of the simulation to the ones derived with the simple model for a run with the LS220/NSE EOS, starting with an initial central density of $5 \times 10^{10} \text{ g cm}^{-3}$, uniform entropy of $1.45 k_B^{-1}$ and $Y_e(0) = 0.4$. The mass with positive energy is being ejected. The entropy change shows how well the shock strength is described by the model, since it is independent of the hydrostatic equilibrium constraint, unlike the other parameters, such as density and pressure. The ejected mass of this run is $0.0517M_\odot$, while the model gives a mass of $0.0537M_\odot$, about $\sim 4\%$ difference. The deviation in the density and entropy profiles between the model and the simulation are less than 2% in density and less than 20% in entropy, except for the model's last part, $10^{-3}M_\odot$ from the edge, where the entropy quickly rises.

6 CONCLUSIONS

In this work, we implemented a numerical scheme to accurately calculate the amount of ejected mass following AIC. We assumed a spherical collapse and neglected neutrinos and GR corrections. We found the amount of ejected mass to be few $\times 10^{-2}M_\odot$ for a large range of initial conditions and EOS, and, as expected, to always move at mildly relativistic

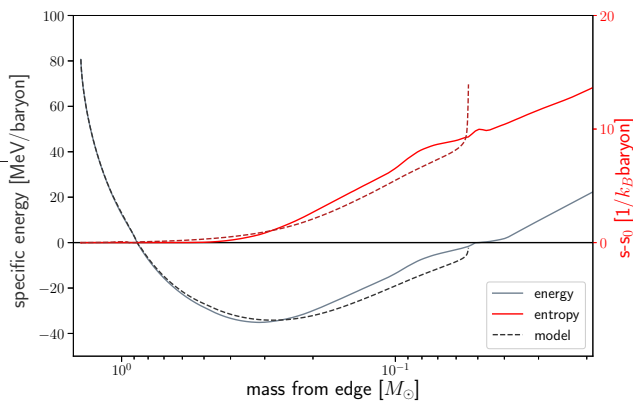


Figure 5. Results of the simulation (solid lines) and the model (dashed lines) for the energy and entropy as a function of the mass from the edge of the star. For the simulation, we used the LS220/NSE EOS, initial entropy per baryon of $1.45 k_B^{-1}$ and $Y_e(0) = 0.40$. Plotted are the total specific energy (gray) and the change in the initial entropy (red). The ejected mass of the simulation is the mass where the energy becomes positive, and for the model it is simply where the curve ends. The model predicts the ejected mass to an accuracy of $\sim 4\%$. The deviation of the entropy and energy between the simulation and model are less than 20%.

velocities. We have suggested a simple model that estimates the ejected mass at the end of the AIC to within 15% given two free parameters, while describing the PNS structure to reasonable accuracy ($< 2\%$ in density and $< 20\%$ in entropy). Our numerical scheme can serve as a basis for future studies, where more physical aspects can be taken into account and integrated into the scheme.

Waxman (2017) suggested that the persistent radio source, associated with FRB 121102, can be explained by the propagation of a spherical shell of plasma into a surrounding medium. The properties of the persistent source imply that the mass of the shell is $\sim 10^{-5} M_\odot$ moving at mildly relativistic velocities, for a duration of $t < 10^{2.5}$ yr. This suggests that the source was created by a weak stellar explosion, such as AIC, since the mass of the shell is much smaller than the ejecta mass from a typical supernova. The obtained ejected mass of $\sim 10^{-2} M_\odot$ is larger than the estimated ejected mass shell of the FRB 121102 persistent source ($\sim 10^{-5} M_\odot$). This inconsistency could be a result of the neglected physical processes, such as neutrino physics, GR corrections and rotation, or non-representative initial conditions. A preliminary neutrino emission calculation did reduce the ejecta mass by an order of magnitude, but not down to $\sim 10^{-5} M_\odot$. Future work could determine more reliably the connection between the persistent source of FRB121102 and the AIC process.

ACKNOWLEDGEMENTS

We thank Eddie Baron, Boaz Katz, Eran Ofek, and Eli Waxman for useful discussions. DK is supported by the Israel Atomic Energy Commission and The Council for Higher Education and Pazi Foundation and by a research grant from The Abramson Family Center for Young Scientists.

REFERENCES

- Bethe H. A., 1990, *Reviews of Modern Physics*, 62, 801
 Canal R., Isern J., Labay J., 1980, *ApJL*, 241, L33
 Chabrier G., Potekhin A. Y., 1998, *Physical Review E*, 58, 4941
 Chatterjee S., et al., 2017, *Nature*, 541, 58
 Cyburt R. H., et al., 2010, *ApJS*, 189, 240
 Dessart L., Burrows A., Ott C. D., Livne E., Yoon S.-Y., Langer N., 2006, *ApJ*, 644, 1063
 Drout M. R., et al., 2014, *ApJ*, 794, 23
 Fryer C., Benz W., Herant M., Colgate S. A., 1999, *ApJ*, 516, 892
 Itoh N., Hayashi H., Nishikawa A., Kohyama Y., 1996, *ApJS*, 102, 411
 Kushnir D., 2018, *MNRAS*, 483, 425
 Lattimer J. M., 2012, *Annual Review of Nuclear and Particle Science*, 62, 485
 Lattimer J. M., Swesty F. D., 1991, *Nuclear Physics A*, 535, 331
 Liebendörfer M., 2005, *ApJ*, 633, 1042
 Livne E., 1993, *ApJ*, 412, 634
 Lyne A., Manchester R., D’Amico N., 1996, *ApJL*, 460, L41
 Lyutikov M., Toonen S., 2018, arXiv preprint arXiv:1812.07569
 Nomoto K., 1986, *Progress in Particle and Nuclear Physics*, 17, 249
 O’Connor E., Ott C. D., 2010, *Classical and Quantum Gravity*, 27, 114103
 Paxton B., Bildsten L., Dotter A., Herwig F., Lesaffre P., Timmes F., 2010, *ApJS*, 192, 3
 Paxton B., et al., 2015, *ApJS*, 220, 15
 Schneider A. d. S., Roberts L. F., Ott C. D., 2017, *Physical Review C*, 96, 065802
 Scholz P., et al., 2016, *ApJ*, 833, 177
 Shen G., Horowitz C., Teige S., 2011a, *Physical Review C*, 83, 035802
 Shen H., Toki H., Oyamatsu K., Sumiyoshi K., 2011b, *ApJS*, 197, 20
 Timmes F., Arnett D., 1999, *ApJS*, 125, 277
 Waxman E., 2017, *ApJ*, 842, 34
 Woosley S., Baron E., 1992, *ApJ*, 391, 228
 Yahil A., 1983, *ApJ*, 265, 1047

APPENDIX A: NUMERICAL DETAILS

A1 Nuclear reaction network and NSE

Nuclear reactions were calculated with the MESA routines (Paxton et al. 2015). The forward reaction rates are taken from JINA reaclib database (Cyburt et al. 2010). The rates in JINA are only valid up to 10^{10} K, which does not cover the temperature range in our simulations, even for matter that is not in NSE. We therefore used the rate at 10^{10} K for higher temperatures. Backward rates are calculated from detailed balance. We allow the EOS of each numerical cell to change from the MESA routines for ideal gas to NSE/nuclear, and vice versa. When the cell is at the MESA EOS, isotopes approach NSE due to nuclear burning. When the temperature is higher than 5×10^9 K and the mass fraction X_i of every isotope does not differ by more than 0.01 from the NSE composition, the EOS is replaced. The NSE composition is calculated for 3335 isotopes in order to accurately describe the EOS over a wide range of T, ρ, Y_e . In order to have a smooth transition when changing the EOS, it is required that the MESA EOS will contain all isotopes whose NSE composition at transition has non-negligible mass fractions. The list of these isotopes was prepared in the same method as in Kushnir (2018),

by observing the isotopes with a molar mass fraction, $Y_i = X_i/A_i$ larger than 10^{-5} at the range of parameters for which the MESA EOS is relevant, $T \in [2 \times 10^9, 3 \times 10^{10}]$ K, $\rho \in [100, 10 \times 10^{10}]$ g cm $^{-3}$ and $Y_e \in [0.495, 0.5]$. We have found that list NSE5 (with 179) from [Kushnir \(2018\)](#) together with 4 additional isotopes (^{34}P , ^{35}P , ^{62}Ga , ^{65}Ge) is sufficient. As the temperature of a cell in NSE drops below 5×10^9 K, the EOS changes to the MESA EOS, with the composition being the NSE composition at the time of the transition.

A2 Entropy as an EOS variable

At the large densities reached during the simulations, matter is highly degenerate and the temperature is a very sensitive function of the internal energy. Since the temperature is used in all our EOS as one of the input variables, it should be accurately obtained. The dependence of the specific entropy s on the temperature is not a very sensitive function, and thus the entropy, instead of the energy, is used to evolve the EOS quantities, using the second law of thermodynamics:

$$Tds = \delta Q, \quad (\text{A1})$$

with Q being the heat flow (per unit mass) in or out of the system. The heating can be a result of shock, neutrino emission, and nuclear burning. Note that when the composition changes due to nuclear burning, the heat added is the sum of the energy increase due to rest mass difference and chemical potential times the composition difference:

$$\delta Q_{nuc} = de - \sum_i \mu_i dy_i. \quad (\text{A2})$$

In NSE, matter reaches thermal equilibrium with respect to nuclear reactions and these terms cancel each other out, such that the entropy no longer changes due to nuclear reactions.

A3 Neutrino physics

Although neutrino physics has an important role at the large densities and temperatures that take place in the AIC process, it is only partly considered in this work. In order to give a lower bound to the ejected mass, we omit the interaction of the neutrinos after creation and assume they freely escape the star, reducing the energy and entropy as a result. We consider two processes - deleptonization due to electron capture and creation of thermal neutrino-anti neutrino pairs. To account for deleptonization, we use the prescription of [Liebendörfer \(2005\)](#), in which the electron fraction Y_e is determined from the instantaneous density alone. This prescription was calibrated from a full calculation and is relevant only until bounce, so we let the Y_e profile freeze afterwards. Entropy loss is calculated by ([Bethe 1990](#)):

$$Tds = -\delta y_e \left(\frac{1}{6} \mu_e - (\mu_n - \mu_p) \right), \quad (\text{A3})$$

where $\mu_{\{e,n,p\}}$ is the chemical potential of the electrons, neutrons and protons, respectively.

Creation and emission of thermal neutrinos is calculated from the expressions of [Itoh et al. \(1996\)](#), where the energy loss rate per unit mass is given as a function of the density, temperature, mean number of nucleons \bar{A} , and mean charge

\bar{Z} . Since we assume the composition does not change in this process, the energy loss is entirely converted to heat loss.

APPENDIX B: COMPARISON TO ANALYTIC SOLUTION

In order to test our numerical scheme, we compared it with the self-similar analytic solution of [Yahil \(1983\)](#) for the collapse of a spherically symmetric star with a polytropic equation of state:

$$p = \kappa \rho^\gamma, \quad (\text{B1})$$

for the adiabatic index $6/5 \leq \gamma \leq 4/3$. The solution uses the self-similar dimensionless coordinate

$$X = r/r_0(t), \quad r_0(t) = \kappa^{1/2} G^{1-\gamma/2} (t_c - t)^{2-\gamma}. \quad (\text{B2})$$

The interval from the catastrophe time $t_c - t$ determines the scaling of the physical variables (coordinate, velocity, etc.) to the self-similar ones. This interval is unknown during the simulation, and is computed by best fitting to the analytic solution. Figure B1 shows the velocity and density during the collapse of a star with an ideal gas EOS with $\gamma = 1.3$, normalized to the self-similar variables, done with a resolution of 2000 cells, initially divided with equal radial spacing. The self-similar solution is plotted on top for comparison. The agreement is within 6% over a range of 10 orders of magnitude. A convergence test we have performed shows that the deviation between the simulation and the analytic solution is (roughly) inversely proportional to the resolution.

This paper has been typeset from a $\text{\TeX}/\text{\LaTeX}$ file prepared by the author.

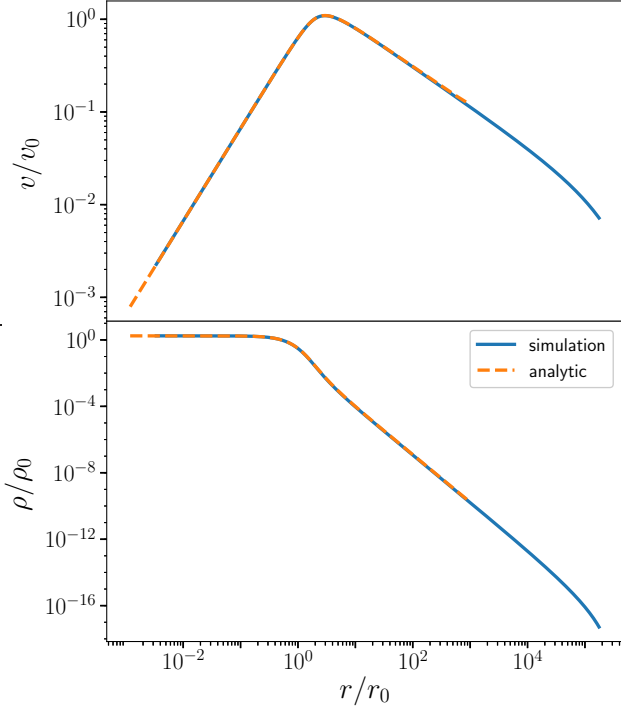


Figure B1. The simulated (blue) infall velocity (upper plot) and density (lower plot) during the simulation of the collapse of an ideal gas polytrope with an adiabatic constant $\gamma = 1.3$ as a function of distance from the center, compared to the analytic self-similar solution (red). All quantities are dimensionless, where the values given by the simulation are normalized by the self-similar scaling.